Journal of Power Sources 196 (2011) 7203–7208

Contents lists available at ScienceDirect

Journal of Power Sources

journal homepage: www.elsevier.com/locate/jpowsour

Degradation of anode supported cell (ASC) performance by Cr-poisoning

Michael Kornely[a,*], Anita Neumann[c], Norbert H. Menzler[c], André Leonide[a], André Weber[a], Ellen Ivers-Tiffée[a,b]

[a] Institut für Werkstoffe der Elektrotechnik (IWE), Karlsruher Institut für Technologie (KIT), Adenauerring 20b, 76131 Karlsruhe, Germany
[b] DFG Center for Functional Nanostructures (CFN), Karlsruhe Institute of Technology (KIT), 76131 Karlsruhe, Germany
[c] Forschungszentrum Jülich (FZJ), Institute of Energy Research (IEF-1), 52428 Jülich, Germany

ARTICLE INFO

Article history:
Received 31 July 2010
Received in revised form
21 September 2010
Accepted 12 October 2010
Available online 20 October 2010

Keywords:
SOFC
LSM
Cr-poisoning
Degradation
Metallic interconnector (MIC)
Distribution of relaxation times (DRT)

ABSTRACT

Performance and stability of solid oxide fuel cells (SOFC) have been continuously improved at the single-cell level. Connecting the individual cells by a metallic interconnector (MIC) in a stack, though, yields remarkable losses in performance and leads to an enhanced degradation. These effects are attributed to, inter alia, Cr evaporation from the MIC and, thus, Cr poisoning of the cathode.

To determine the degradation rate caused by Cr poisoning, this paper focuses on the differences in single cell performance and short-term stability by using either an inert flowfield or a flowfield made of a chromia-forming alloy. To provide a homogeneous current collection and gas distribution over the complete cathode area and to avoid a direct contact between MIC made of Crofer22APU and LSM, a platinum mesh was used as current collector. The cell performance was evaluated by analyzing its current–voltage characteristics and using electrochemical impedance spectroscopy.

A detailed analysis of impedance spectra by the distribution of relaxation times (DRT) and a subsequent Complex Nonlinear Least Squares (CLNS) fit facilitated the separation of anodic and cathodic polarization processes. In the presence of a chromia-forming alloy the polarization resistance of the cathode showed a significantly higher initial value (+64 $m\Omega \cdot cm^2$) than without and a high degradation rate of 213 $\mu\Omega \cdot cm^2\ h^{-1}$ during 280 h of galvanostatic operation at 800 °C.

1. Introduction

The performance of solid oxide fuel cells (SOFC) at the single-cell level has been continuously improved over the past 10 years [1]. However, at the stack level, the power density decreases by 50% and becomes unprofitable [2]. A search for the causes leads to the part of the metallic interconnector (MIC): Apart from additional losses caused by the MIC geometry [3], chromium poisoning of the cathode [4] reduces the cell performance.

Poisoning of the cathode by gaseous chromium species is considered one of the major sources of SOFC degradation [5]. Chromium vaporizes from the oxide scale of chromium-containing interconnectors in quantities which depend on SOFC operation temperatures [6]. However, protection coatings can significantly reduce the chromium partial pressure in the cathode gas phase and decelerate the cell degradation [7].

Chromium poisoning of (La,Sr)MnO_3 (LSM) cathodes has been studied extensively [8], but the degrading mechanism still needs to be clarified. Hilpert et al. proposed an electrochemical reduction of chromium species that leads to the formation of solid chromia at the electrochemically active cathode sites, thus blocking them for further oxygen reduction [9]. Jiang et al. rather assumed a purely chemical nucleation and nuclei growth mechanism that forms an additional layer which hinders the diffusion of oxygen ions from the triple phase boundaries (TPB) into the zirconia electrolyte [10]. In case of LSM cathodes Mn^{2+} ions formed under cathodic polarization act as nucleation agent [10]. Recent investigations found that there is no simple correlation between the amount of chromium deposited in the cell and the degradation caused by it [11,12]. So far, no studies are available which differentiate between Chromium poisoning effects at open cell voltage (OCV, without current load) and at galvanostatic conditions (with current load).

Electrochemical impedance spectroscopy (EIS) has been widely used to study the oxygen reduction reaction in SOFC cathodes [13]. In case of LSM cathodes two distinct contributions to the overall polarization resistance in the high and low frequency range have been identified [14]. Both processes are deeply affected by the presence of a chromium source. The low frequency arc associated with the adsorption and diffusion of oxygen on the LSM surface is dominated by the gaseous state of the chromium species. In contrast, the high frequency part which is attributed to either the charge transfer or the oxygen ion migration and diffusion into the

* Corresponding author. Tel.: +49 721 6088456; fax: +49 721 6087492.
E-mail address: michael.kornely@kit.edu (M. Kornely).

0378-7753/$ – see front matter © 2010 Elsevier B.V. All rights reserved.
doi:10.1016/j.jpowsour.2010.10.033

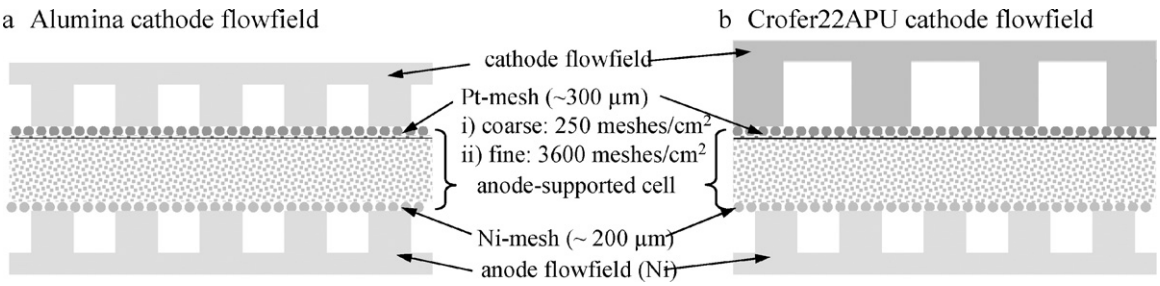

Fig. 1. Two different cathode flowfield materials were applied in this study: (a) Al_2O_3 (Cr-free) and (b) chromia-forming alloy Crofer22APU (Cr-source) to investigate the degradation of ASC performance by Cr-poisoning

zirconia electrolyte lattice is affected by the deposited chromium species [15]. An additional high frequency arc at low operation temperatures has also been observed but its physical origin is so far unknown [15].

2. Experimental

In this study anode-supported cells (ASC) manufactured at Forschungszentrum Jülich were applied. The cells consist of a 50 mm × 50 mm Ni/8YSZ anode substrate (8YSZ: 8 mol% Y_2O_3 doped ZrO_2) and an anode functional layer (Ni/8YSZ-cermet) followed by a gas-tight electrolyte (8YSZ) [16]. Subsequently, a double-layered $La_{0.65}Sr_{0.3}MnO_3$/8YSZ (functional layer)/LSM (current collector) cathode was applied by screen-printing and sintering. Details of the manufacturing procedures of the LSM cathode can be found in [17]. The active area of the working cathode was 10 mm × 10 mm. Two auxiliary (open circuit voltage (OCV) probe) electrodes were applied in gas-flow direction in front of and behind the cathode [18]. The cells were tested in a single-cell test bench [19] and characterized by current–voltage (C–V)- and EIS measurements.

Fig. 1 displays the single cell test setup. The anode substrate was contacted by a nickel contact mesh welded on a Ni-flowfield. The cathode was contacted by a platinum contact mesh. At the cathode, two different flowfield materials were used: (a) Al_2O_3 (providing Cr-free conditions) or (b) commercially available chromia-forming alloy (Crofer22APU, ThyssenKrupp, Cr source). These two different cathode flowfield materials were applied in this study to investigate the degradation of ASC performance by Cr poisoning via gaseous species. In both cases (a and b) the Pt contact mesh was used to provide a homogeneous current collection and gas distribution over the whole cathode area and to avoid a direct contact between Crofer22APU and LSM. Despite of its lower contact resistance [19] an Au mesh was not applied because of an enhanced corrosion and Cr evaporation at the Au-Crofer22APU contact [4]. By using a Pt mesh at the cathode side and a Ni mesh at the anode side, respectively, any contact resistance due to corrosion or interdiffusion was avoided.

The cells were operated under ambient pressure with air at the cathode side and varying H_2O/H_2 mixtures at the anode side. The total anodic and cathodic gas flow rates were maintained at a constant value of 250 ml min^{-1} during all experiments, resulting in a negligible fuel and oxidant utilization. The cells were tested at an operating temperature of 800 °C. The cell performance was evaluated by current–voltage (C–V) characteristics and during a galvanostatic test. Electrochemical impedance spectroscopy (EIS) was performed under open-circuit conditions with a Solartron 1260 frequency response analyzer in a frequency range from 500 mHz to 1 MHz. The amplitude of the current stimulus was adjusted in order to achieve a voltage response not higher than 12 mV. This procedure leads to a good signal-to-noise ratio (SNR) of the measured data and fulfils the condition of linearity in the operating point. The EIS and CV measurements were carried out before (t_1 = 32 h) and after (t_2 = 320 h) a galvanostatic short-term test. Between both measurements the cell was operated at a constant current load of 500 mA cm^{-2} for ~280 h. Within the first 32 h (t = 0 h to the first measurement at t_1 = 32 h) the cells were heated up and operated at OCV-conditions for 10 h at 850 °C and another 12 h at 800 °C. This initial annealing procedure simulates the sealing and the reduction process during the fabrication of a stack.

3. Results and discussion

Fig. 2 shows the power density at 500 mA cm^{-2} of the ASC in case of an Al_2O_3 and a chromia-forming alloy flowfield at the cathode. The power densities were determined at t_1 and t_2. During the galvanostatic test the power density increases about 0.3% in the absence of chromium ($P_{Cr\text{-}free\_t1}$ = 465 mW cm^{-2}, $P_{Cr\text{-}free\_t2}$ = 467 mW cm^{-2}). In the presence of a chromia-forming alloy a considerable decrease of 5% was determined ($P_{Cr\text{-}source\_t1}$ = 438 mW cm^{-2}, $P_{Cr\text{-}source\_t2}$ = 416 mW cm^{-2}). The initial (t_1) power density in case of the chromia-forming alloy flowfield is 6% smaller than for the Cr-free setup with an alumina flowfield. After the galvanostatic test (t_2) a total power decrease of 11% was observed in the presence of chromium, as compared to the Cr-free setup.

To evaluate the physical origins of the strong power degradation caused by the chromia-forming alloy, impedance spectra were measured before and after the galvanostatic test (Fig. 6a and b). It is obvious that the area-specific ohmic resistance (ASR_0: high

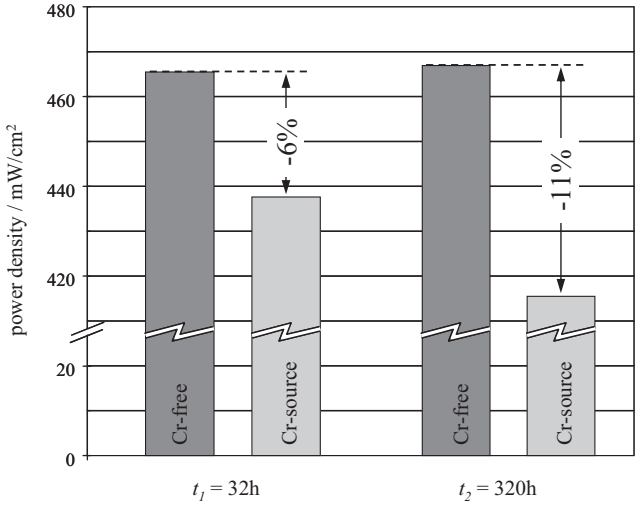

Fig. 2. Power densities of ASCs in case of Al_2O_3 (Cr-free) and Crofer22APU (Cr-source) flowfield at the cathode side (T = 800 °C, current density = 500 mA cm^{-2}, oxidant: air, fuel: H_2, 3.4% H_2O). The power densities were determined at the beginning (t_1) and at the end (t_2) of a galvanostatic short-term test (280 h at 500 mA cm^{-2}).

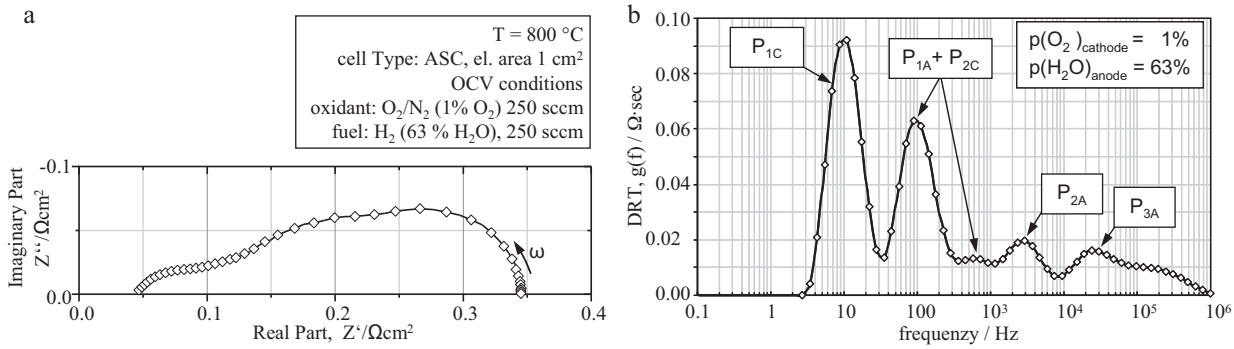

Fig. 3. (a) Impedance spectra of an anode supported cell with LSM cathode measured at $p(O_2)_{cathode}$ = 1% and $p(H_2O)_{anode}$ = 63% and (b) corresponding distribution of relaxation times (DRT). Unlike the Nyquist plot, a last 5 processes are visible in the distribution curve.

frequency intercept, Fig. 3a) as well as the area-specific polarization resistance (ASR_{pol}: difference between low and high frequency intercept, Fig. 3a) are influenced by the flowfield. The small difference in ASR_0 has to be attributed to the difference in flowfield geometry [3]. The significant difference in ASR_{pol} as well as the ASR_{pol} degradation which was observed in case of a chromia-forming alloy as the cathode flowfield have been investigated in detail.

The anodic and cathodic polarization losses contained in the impedance data sets were evaluated using the commercially available complex nonlinear last square (CNLS) fit software Z-View®. The applied equivalent-circuit model was derived from a pre-identification of the impedance response by calculating and analyzing the corresponding distribution of relaxation times (DRT) [18,21,20,22].

The higher resolution of the DRT renders possible the identification of losses with characteristic frequencies separated by only half a decade as demonstrated by the comparison of the impedance spectrum (Fig. 3a) and the corresponding DRT (Fig. 3b) of the ASC under investigation. Unlike the impedance curve where the individual polarization processes overlap, at least four processes (P_{1C}, P_{1A}, P_{2C}, P_{2A}, and P_{3A}) can be clearly distinguished in the calculated DRTs. Particular attention should be paid to process P_{1A}. Characteristic of this process are its two peaks in the DRT at around 100 Hz and 600 Hz [20].

The detailed equivalent circuit (Fig. 4c) resulting from the analysis of the DRTs consists of 6 serial impedance elements, each characteristic of one loss mechanism: (i) an ohmic resistor (overall ohmic losses), (ii) 2 serial RQ elements (P_{2A} and P_{3A}: gas diffusion coupled with activation polarisation and ionic transport in the anode functional layer) [18,20,22], (iii) a Gerischer element (P_{2C}: oxygen surface exchange kinetics and oxygen diffusivity in the bulk of the cathode), (iv) a generalized finite length Warburg Element (G-FWS) (P_{1A}: diffusion polarisation in the anode substrate), and (v) an RQ element (P_{1C}: diffusion polarisation in the cathode), cf. Table 1. With the help of this equivalent-circuit model, the measured impedance spectra could be separated into the single loss contributions (Fig. 3a), thus permitting a precise determination of the area-specific resistance values for the single loss contributions of the investigated ASCs.

In Fig. 4b the distribution of relaxation times (DRT) of the cell contacted with a Pt mesh and an Al_2O_3 flowfield is shown for 3.4% H_2O and 63% H_2O in the fuel gas (H_2), respectively. The anode processes P_{3A} and P_{2A} (each modelled by a resistance in parallel to a constant phase element, relaxation frequency ~20 kHz and ~1 kHz) are clearly visible. The gas diffusion process P_{1A} in the anode sub-

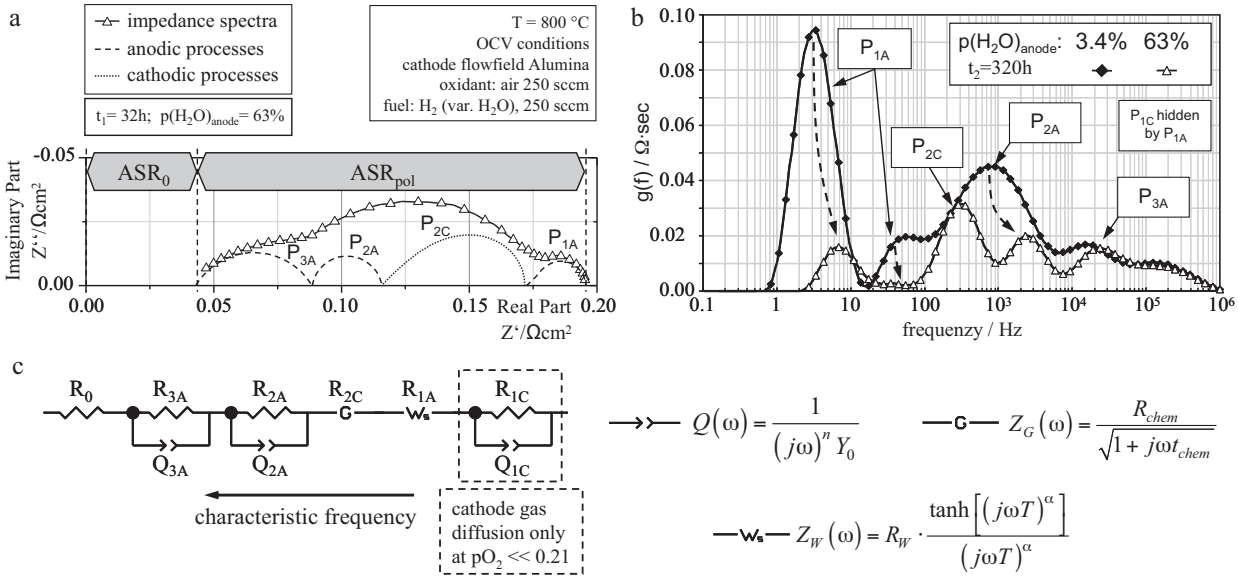

Fig. 4. (a) Measured impedance data shows the ASR_0 and ASR_{pol} for alumina flowfield (Cr-free) carried out before (t_1) a galvanostatic short-term test (~280 h at 500 mA cm^{-2}) and a example for CNLS fit of the anodic and cathodic polarization losses. (b) Distribution of relaxation times (DRT) corresponding to measured impedance data for alumina flowfield (Cr-free) carried out at the end (t_2) of the galvanostatic short-term test at different $p(H_2O)_{anode}$ = (i) 3.4% and (ii) 63%, (c) and equivalent circuit model used for the CNLS-fit to describe ohmic anode and cathode polarization losses.

Table 1
List of the circuit elements of the applied ECM, together with their temperature, gas partial pressure and frequency dependencies as well as the magnitude of the real part of the according resistance (T = 800 °C, OCV-conditions, oxidant: air, fuel: H_2, 63% H_2O).

Process	Element	f_r, ASR	Dependencies	Parameters	Physical origin
R_0	R_0	44–64 mΩ·cm²	Temperature	R_0	Ohmic resistance (electrolyte)
P_{1C}	RQ	0.3–10 Hz, 4 mΩ·cm²	pO_2, temperature (low)	Y_{1C}, n_{1C}	Gas diffusion in the pores of the cathode structure
P_{2C}	Gerischer	10–1 kHz, 56–185 mΩ·cm².	$R_{2C} \propto pO_2^{-0.22}$, temperature	R_{chem}, t_{chem}	Oxygen surface exchange kinetics and O^{2-}-diffusivity in the cathode bulk material
P_{1A}	GFLW	2–20 Hz, 23–25 mΩ·cm²	pH_2, pH_2O, temperature (low)	R_{1A}, τ_{1A}, n_{1A}	Gas diffusion in the anode substrate
P_{2A}	RQ	200 Hz–10 kHz, 21–26 mΩ·cm²	pH_2, pH_2O,temperature	Y_{2A}, n_{2A}	(P_{2A} + P_{3A}) gas diffusion coupled with charge transfer reaction and ionic transport in the anode functional layer (AFL)
P_{3A}	RQ	6–80 kHz, 42–44 mΩ·cm²	pH_2, pH_2O, temperature $R_{2A} + R_{3A} \propto pH_2^{0.10}$, $R_{2A} + R_{3A} \propto pH_2O^{-0.33}$	Y_{3A}, n_{3A}	

strate (Warburg element, relaxation frequency ~3 Hz) hides the gas diffusion process P_{1C} at the porous LSM/8YSZ cathode (relaxation frequency ~8 Hz). Due to its low resistance (~3.6 mΩ·cm² in air) [3], the process P_{1C} was fixed during the fitting procedure. At low $p(H_2O)_{anode}$, which is given for 3.4% H_2O, the second peak of the gas diffusion process P_{1A} and the anode process P_{2A} overlap and cover the cathode process P_{2C} (relaxation frequency ~300 Hz), whereas at 63% H_2O the process P_{2C} becomes visible. Hence, by applying well-selected operating conditions, namely a high $p(H_2O)$ at the anode, the cathode polarization resistance R_{2C} can be determined with a high accuracy.

The oxygen reduction reaction within the LSM/8YSZ composite cathode (P_{2C}) is described by a Gerischer element (Fig. 4c), which usually models the oxygen reduction reaction (surface exchange) coupled with oxygen-diffusion in a mixed ionic–electronic conducting cathode ($La_{0.6}Sr_{0.4}Co_{0.2}Fe_{0.8}O_{3-\delta}$: LSCF) [23]. In our case, the oxygen reduction reaction, taking place at the three phase boundaries in the LSM/8YSZ composite, is coupled with the O^{2-} transport in the ionic conducting 8YSZ matrix. Even though we have recommended to describe coupled processes by more complex transmission line models [20], the Gerischer element helps further with a higher stability in the fitting procedure. In Fig. 5a) the residuals of the fit at t_1 for a Crofer22APU (Cr-source) flowfield determine a relative error < 1.9% (in the frequency range 10 Hz to 320 kHz). The Kramers–Kronig validation for the corresponding measured impedance spectrum is shown in Fig. 5b). Noteworthy, the relative errors of both real and imaginary part are below 0.4% for the most part of the spectrum, which is a strong indication for high quality measurement data. The small but still visible mismatch is caused by the CNLS fit of the equivalent circuit model, which was developed for ASC cells with LSCF cathode [20,24]. The error value in the frequency range of process P_{2C} is slightly higher (1.9% for LSM/YSZ versus 0.5% for LSCF) and probably caused by the Gerischer element instead of a transmission line model, which describes the LSM/8YSZ composite cathode more precisely.

The impedance spectra, the corresponding DRTs and the ASR-contributions of the individual processes are displayed in Fig. 6 for an inert Al_2O_3 flowfield (Cr-free, Fig. 6 a, c, and e) and a chromia-forming alloy (Crofer22APU, Fig. 6 b, d, and f) before and after the galvanostatic short-term test. (Between both measurements the cell was operated at a constant current load of 500 mA cm^{-2} for ~280 h). The DRT analysis (Fig. 6c and d) shows the degradation of the cell and in particular the change in ASR_{pol} in a frequency range between 10 Hz and 1 kHz. The relative error with a value < 0.7% (frequency range 70 mHz to 1.1 kHz) between the two measurements is rather small. This is a precondition to determine the influence of gaseous Chromium species on the LSM/YSZ cathode with a sufficient accuracy by using a Gerischer element.

The total area specific polarization resistance ($ASR_{pol} = R_{1A} + R_{2A} + R_{3A} + R_{1C} + R_{2C}$) shows a considerable dependency on the applied flowfield materials and testing time. Comparing the initial ASR_{pol} at t_1 = 32 h of the cells operated with an alumina flowfield ($ASR_{pol,Cr\text{-}free\_t1}$ = 151 mΩ·cm²) with the cells operated with a chromia-forming alloy flowfield

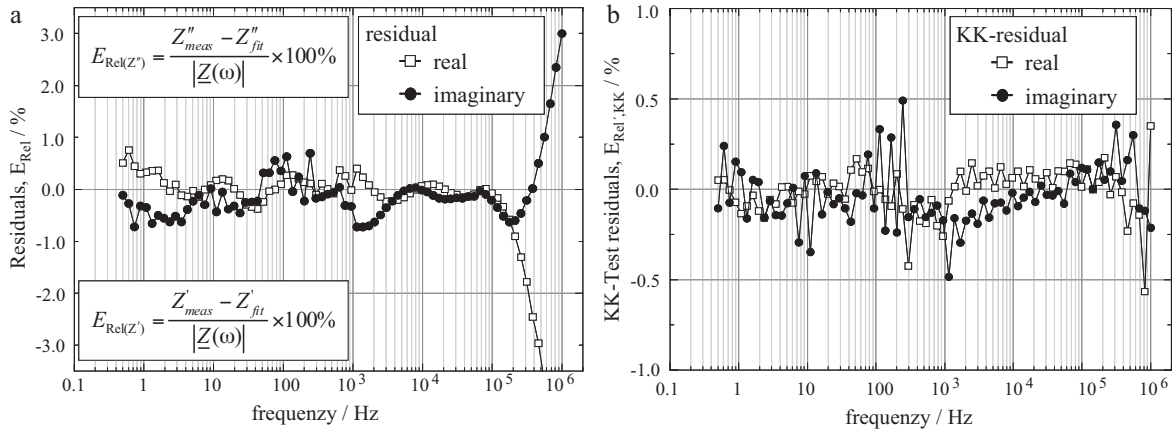

Fig. 5. (a) Residual pattern of the fit at t_1 for Crofer22APU (Cr-source) flowfield at cathode side, and (b) Kramers–Kronig test residuals of the measured impedance spectrum (T = 800 °C, OCV-conditions, oxidant: air, fuel: H_2, 63% H_2O).

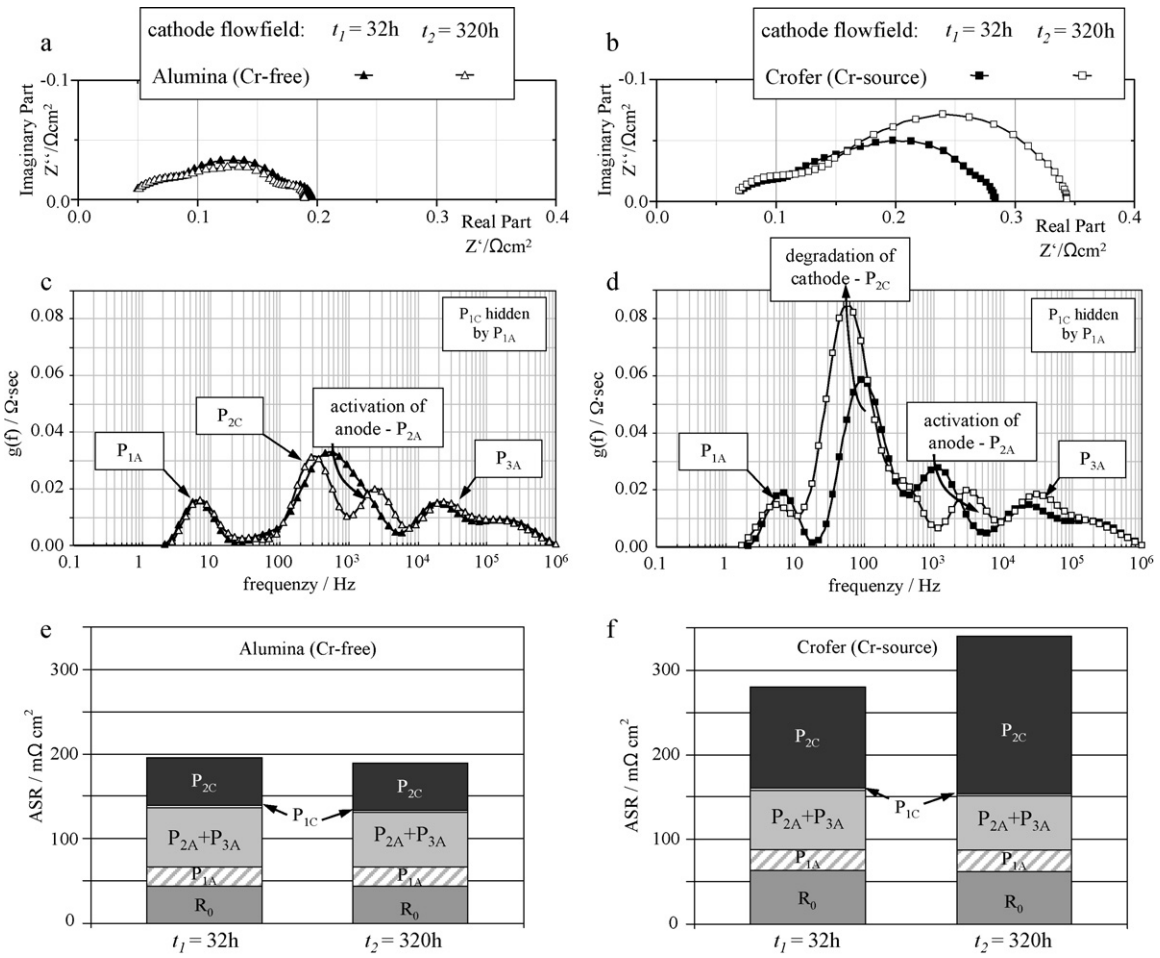

Fig. 6. Electrochemical impedance spectra (EIS) of ASCs with (a) an Al_2O_3 (Cr-free) and (b) Crofer22APU (Cr-source) flowfield at cathode side. The EIS were recorded under OCV conditions (T = 800 °C, oxidant: air, fuel: H_2, 63% H_2O) before (t_1) and after (t_2) a galvanostatic test (280 h at 500 mA cm^{-2}). Distribution of relaxation times corresponding to the impedance data for both cathode flowfield materials: (c) Al_2O_3 (Cr-free) and (d) Crofer22APU (Cr-source). Ohmic and individual polarization losses for (e) Al_2O_3 (Cr-free) and (f) Crofer22APU (Cr-source) flowfield at the cathode side (T = 800 °C, OCV-conditions, oxidant: air, fuel: H_2, 63% H_2O).

($ASR_{pol,Cr\text{-}source\_t1}$ = 217 mΩ·cm^2), a 44% higher initial polarization resistance (ΔASR_{pol_t1} = +66 mΩ·cm^2) is observed for the latter case. Hereby, an increase in polarization resistance originating from chromium poisoning, is quantitatively ascribed to a fixed startup procedure of a single ASC cell and can be transferred to a stack. More details on the early interaction between Fe-Cr alloy metallic interconnect and Sr-doped LaMnO3 cathodes are given in [25]. Jiang et al. confirm that chemical interactions between volatile Cr species and LSM cathodes take place at open voltage conditions, especially in the first hours.

During the galvanostatic short-term test the polarization resistance decreases by 3.2% ($\Delta ASR_{pol,Cr\text{-}free}$ = −4.8 mΩ·cm^2) in the absence of chromium. In contrast, a notable increase of 28% ($\Delta ASR_{pol,Cr\text{-}source}$ = +60 mΩ·cm^2) is observable in the presence of the chromia-forming alloy.

A comparison of the individual polarization processes at the anode and cathode shows that the initial values (t_1) of the anode processes P_{1A} (R_{1A} = 23 . . . 25 mΩ·cm^2), P_{2A} (R_{2A} = 26 mΩ·cm^2) and P_{3A} (R_{3A} = 43 mΩ·cm^2) are not affected by the cathode flowfield. During the galvanostatic short-term test P_{2A} decreased (ΔR_{2A} = −4 . . . −5 mΩ·cm^2) whereas P_{1A} and P_{3A} did not change. More information about the activation effect of P_{2A} can be found in [20] and [24].

The difference in the initial ASR_{pol} is related to the polarization resistance of the cathode (R_{2C}). The initial R_{2C} in case of a chromia-forming alloy flowfield exceeds the R_{2C} in case of a Cr-free flowfield by 115% (ΔR_{2C_t1} = +64 mΩ·cm^2). Whereas P_{2C} decreased during the galvanostatic short-term test ($\Delta R_{2C,Cr\text{-}free}$ = −1.2 mΩ·cm^2) in a chromium-free environment, an increase of 54% was observed in case of a chromia-forming alloy flowfield ($\Delta R_{2C,Cr\text{-}source}$ = +65 mΩ·cm^2). These results clearly show that the presence of a chromium source results in a significant increase of the polarization resistance of the LSM cathode. Already during the start-up of the cell a significant chromium poisoning takes place (ΔR_{2C} = +64 mΩ·cm^2 within 10 h at 850 °C + 12 h at 800 °C) and continues during cell operation (ΔR_{2C} = +130 mΩ·cm^2 within ∼280 h at 800 °C). The high initial degradation rate during the start-up of the cell (3.2 mΩ·cm^2 h^{-1}) might be related to the higher temperature (850 °C for 10 h). The difference in R_{2C} at t_1 clearly shows that chromium poisoning also takes place under OCV-conditions, where the electrochemical reduction of chromium species at the three phase boundary does not occur. The initial degradation during the start-up procedure (3.2 mΩ·cm^2 h^{-1}) as well as during the galvanostatic short-term test (213 μΩ·cm^2 h^{-1}), is far above tolerable limits. This comparative study clearly indicates that the development and application of long-term stable protective coatings is indispensable for a reliable stack operation.

4. Conclusions

The degradation rate caused by Cr-evaporation from a metallic interconnector source was investigated on anode supported type

SOFC single cells. For this purpose, ASC cell initial performance (~32 h) and short-term stability (~320 h) was determined using either an inert material (Al_2O_3) or a chromia-forming alloy (Crofer22APU) at the cathode side of the interconnector. In both cases, a Pt mesh between the cathode surface and the interconnector flow-field provided a homogenous current density and gas distribution over the entire cell area.

Only in the presence of a chromia-forming alloy the polarization resistance of the cathode showed a severe degradation of +64 $m\Omega \cdot cm^2$ during the first 32 h at OCV conditions, and another +66 $m\Omega \cdot cm^2$ within 280 h of galvanostatic operation. For the first time, it was proven that the presence of chromium species in the cathodic gas phase deteriorates the cell performance already at OCV conditions. This result clearly indicates that the electrochemical reduction of chromium species at the three-phase boundary is not the unique degradation effect originating from metallic interconnector materials. Overall, the metallic interconnector (without protective coating) was responsible for a degradation rate of 213 $\mu\Omega \cdot cm^2\ h^{-1}$, whereas the inert ($Al_2O_3$) interconnector leads to a decrease of 5 $m\Omega \cdot cm^2$ during 280 h of galvanostatic operation at 800 °C.) In total, a power decrease of 11 % was observed for the ASC cell in the presence of gaseous chromium species at the cathode side, as compared to a Cr-free environment. This comparative study proves that long-term stable protective coatings are indispensable for a reliable stack operation, valid both for auxiliary power (APU) and stationary application.

Acknowledgement

Financial support by the Bundesministerium für Wirtschaft und Technologie (BMWi) and the BMW Group in Munich (project ZeuS III, FKZ 0327766D) is gratefully acknowledged. The authors wish to express their thanks to Jan Philipp Schmidt and Stanley Jose from IWE for their support.

References

[1] F. Tietz, V.A.C. Haanappel, A. Mai, J. Mertens, D. Stöver, Journal of Power Sources 156 (2006) 20–22.
[2] L. Blum, W.A. Meulenberg, H. Nabielek, R. Steinberger-Wilckens, International Journal of Applied Ceramic Technology 2 (2005) 482–492.
[3] M. Kornely, A. Weber, E. Ivers-Tiffée, Proceedings of 9th European Solid Oxide Fuel Cell Forum, Vol. 16, 2010, pp. 54–65.
[4] M.C. Tucker, H. Kurokawa, C.P. Jacobson, L.C. De Jonghe, S.J. Visco, Journal of Power Sources 160 (2006) 130–138.
[5] V. Wolf, Y. Harumi, A.G. Hubert, High-Temperature Fuel Cells, Handbook of Fuel Cells, John Wiley & Sons Ltd., 2009, pp. 921–931.
[6] M. Stanislowski, E. Wessel, K. Hilpert, T. Markus, L. Singheiser, Journal of Electrochemical Society 154 (2007) A295–A306.
[7] M. Stanislowski, J. Froitzheim, L. Niewolak, W.J. Quadakkers, K. Hilpert, T. Markus, L. Singheiser, Journal of Power Sources 164 (2007) 578–589.
[8] Vielstich Wolf, Yokokawa Harumi, A. Gasteiger Hubert, Durability of Cathodes Including Cr Poisoning, Handbook of Fuel Cells, John Wiley & Sons Ltd., 2009, pp. 566–578.
[9] K. Hilpert, D. Das, M. Miller, D.H. Peck, R. Weiss, Journal of Electrochemical Society 143 (1996) 3642–3647.
[10] S.P. Jiang, J.P. Zhang, X.G. Zheng, Journal of the European Ceramic Society 22 (2002) 361–373.
[11] A. Neumann, N.H. Menzler, I. Vinke, H. Lippert, The Electrochemical Society (2009) 2889–2898.
[12] N.H. Menzler, I. Vinke, H. Lippert, The Electrochemical Society (2009) 2899–2908.
[13] E. Ivers-Tiffée, A. Weber, H. Schichlein, Electrochemical impedance spectroscopy, in: W. Vielstich, H.A. Gasteiger, A. Lamm (Eds.), Handbook of Fuel Cells—Fundamentals, Technology and Applications, John Wiley & Sons Ltd., Chichester, 2003, pp. 220–235.
[14] Y. Matsuzaki, I. Yasuda, Solid State Ionics 132 (2000) 271–278.
[15] S.P. Jiang, J.P. Zhang, K. Foger, Journal of Electrochemical Society 147 (2000) 3195–3205.
[16] H.P. Buchkremer, U. Diekmann, D. Stöver, Proceedings of the 2nd European Solid Oxide Fuel Cell Forum, Vol. 1, 1996, pp. 221–228.
[17] V.A.C. Haanappel, A. Mai, J. Mertens, Solid State Ionics 177 (2006) 2033–2037.
[18] A. Leonide, S. Ngo Dinh, A. Weber, E. Ivers-Tiffée, Proceedings of the 8th European Solid Oxide Fuel Cell Forum, 2008, p. A0501T.
[19] A. Weber, A.C. Müller, D. Herbstritt, E. Ivers-Tiffée, Proceedings of the Seventh International Symposium on Solid Oxide Fuel Cells (SOFC-VII), 2001, pp. 952–962.
[20] A. Leonide, V. Sonn, A. Weber, E. Ivers-Tiffée, Journal of Electrochemical Society 155 (2008) B36–B41.
[21] H. Schichlein, A.C. Müller, M. Voigts, A. Krügel, E. Ivers-Tiffée, Journal of Applied Electrochemistry 32 (2002) 875–882.
[22] V. Sonn, A. Leonide, E. Ivers-Tiffée, Journal of Electrochemical Society 155 (2008) B675–B679.
[23] S.B. Adler, J.A. Lane, B.C.H. Steele, Journal of Electrochemical Society 143 (1996) 3554–3564.
[24] C. Endler, A. Leonide, A. Weber, E. Ivers-Tiffée, F. Tietz, ECS Transactions 25 (2009) 2381–2390.
[25] S.P. Jiang, S. Zhang, Y.D. Zhen, Journal of Materials Research 20 (2005) 747–758.